The absorption spectrum of nitrous oxide between 7647 and 7918 cm−1

E.V. Karlovets, S. Kassi, S.A. Tashkun, A. Campargue

The absorption spectrum of nitrous oxide between 7647 and 7918 cm^{-1}

E.V. Karlovets [1,2*], S. Kassi [1], S.A. Tashkun [3] and A. Campargue [1*]

[1] *Univ. Grenoble Alpes, CNRS, LIPhy, 38000 Grenoble, France*
[2] *Tomsk State University, Laboratory of Quantum Mechanics of Molecules and Radiative Processes, 36, Lenin Avenue, 634050, Tomsk, Russia*
[3] *V.E. Zuev Institute of Atmospheric Optics, 1, Academician Zuev square, 634055 Tomsk, Russia*

Number of pages: 24 25 October 2023

Number of tables: 3

Number of figures: 9

Keywords: Nitrous oxide, N_2O, high-resolution spectra, Cavity Ring Down spectroscopy, line positions, line intensities, HITRAN, HITEMP.

* Corresponding authors:
E-mails: alain.campargue@univ-grenoble-alpes.fr (A. Campargue)

Abstract

We revisit the room temperature absorption spectrum of natural nitrous oxide recorded by high sensitivity cavity ring down spectroscopy between 7647 and 7918 cm^{-1} (1.31–1.26 µm) reported by Liu et al. (doi: 10.1016/j.jms.2011.03.025). In this previous analysis, 2272 transitions could be assigned in the region and no intensity information was provided. In the present work, on the basis of improved predictions of the effective operator models, the assignments could be extended to more than 3200 transitions and, more importantly, line intensities are provided for all the transitions. The assigned transitions belong to 49 bands of the $^{14}N_2{}^{16}O$, $^{14}N^{15}N^{16}O$, $^{15}N^{14}N^{16}O$, $^{14}N_2{}^{18}O$, and $^{14}N_2{}^{17}O$ isotopologues, 16 being newly assigned. All the identified bands correspond to the ΔP= 14 series of transitions, except for four ΔP= 12 and two ΔP= 13 bands of the $^{14}N_2{}^{16}O$ isotopologue ($P= 2V_1+V_2+4V_3$ is the polyad number where V_i= 1-3 are the vibrational quantum numbers). For comparison, the HITRAN2020 database includes only the $\nu_1+3\nu_3$ band of the main isotopologue and a number of calculated line parameters for the fourth minor isotopologue, $^{14}N_2{}^{18}O$.

The band-by-band analysis provides accurate spectroscopic parameters of 46 bands from a fit of the measured line positions. Nine resonance perturbations were identified including a few extra lines for two $^{14}N_2{}^{16}O$ bands. The interaction mechanisms and the perturbers were assigned on the basis of the effective Hamiltonian models.

The comparison with current spectroscopic databases (HITRAN, HITEMP, NOSD) is discussed. All show significant deviations compared to the reported results (*e.g.* for ΔP= 13 band intensities). The reported results will be thus valuable to more accurately account for the absorption of nitrous oxide in the region.

1. Introduction

Nitrous oxide is a powerful greenhouse gas with a warming effect power about 300 times stronger than carbon dioxide. Its atmospheric concentration of about 330 ppb is increasing at a rate of about 1 ppb/year. The atmospheric importance of N_2O makes an accurate characterization of its absorption spectrum suitable. We are involved in a long-term project aiming at a study of the high sensitivity absorption spectrum of nitrous oxide by cavity ring down spectroscopy (CRDS) in the near-infrared. **Fig. 1** presents an overview of the spectral intervals studied by CRDS within the last fifteen years. Overall, the 5696-8630 cm^{-1} range was continuously covered by CRDS [1-11]. The HITEMP [12] and HITRAN2020 [13] lists of $^{14}N_2{}^{16}O$ are included in the plot. The HITRAN list corresponds to an intensity cut off of 2×10^{-25} cm/molecule at 296 K *i.e.* about 4 orders of magnitude above the CRDS detectivity threshold. The HITEMP line list for N_2O is a mixture of the NOSD-1000 [21] and HITRAN2016 [22] data. The NOSD-1000 list is a calculated line list with positions obtained using an effective Hamiltonian (EH) model with parameters fitted on experimental positions [14] and intensities computed from effective dipole moments (EDM) with parameters fitted on measured line intensities [15]. In the studied regions, the CRDS studies provide the main source of line positions used to refine the parameters of the EH models. As concerns line intensity calculations, they require a set of EDM parameters for each ΔP value ($P= 2V_1+V_2+4V_3$ is the polyad number where V_i= 1-3 are the vibrational quantum numbers). We have highlighted in **Fig. 1**, the transitions for which intensity information was retrieved from the CRDS spectra. Line intensities were obtained for only part of the recorded CRDS spectra which makes some sets of EDM inaccurate or incomplete and leads to strong deviations between the HITEMP line list and the recorded CRDS spectra (see e.g. Ref. [10].

In the present work, we reconsider the spectral region between 7647 and 7918 cm^{-1}, first analyzed by Liu et al. [7] in 2011. In that work, 2272 transitions could be assigned but no intensity information was provided. Here, using the same spectra, line intensities are systematically retrieved. We have included in the lower panel of **Fig. 1** a review of the intensity information available in the literature in the considered region. It is limited to two studies by Fourier transform spectroscopy (FTS) by Daumont et al. [15] and Toth [16]. The former is the more sensitive. It was performed with an absorption path length of 48.26 m and corresponds to a detectivity threshold of about 10^{-26} cm/molecule, to be compared to a 10^{-29} cm/molecule value for the weakest lines measured by CRDS.

This paper is organized as follows. The experimental setup and the construction of the measured lists are briefly described in Section 2. In Section 3, we present the spectra analysis by comparison with the effective operator predictions which added about 900 new rovibrational assignment transitions compared to Ref. [7]. The band-by-band fitting of the G_v, B_v. D_v, and H_v band parameters and identification of resonance perturbations are presented in Section 4 before the discussion of the comparison with current spectroscopic databases (Section 5).

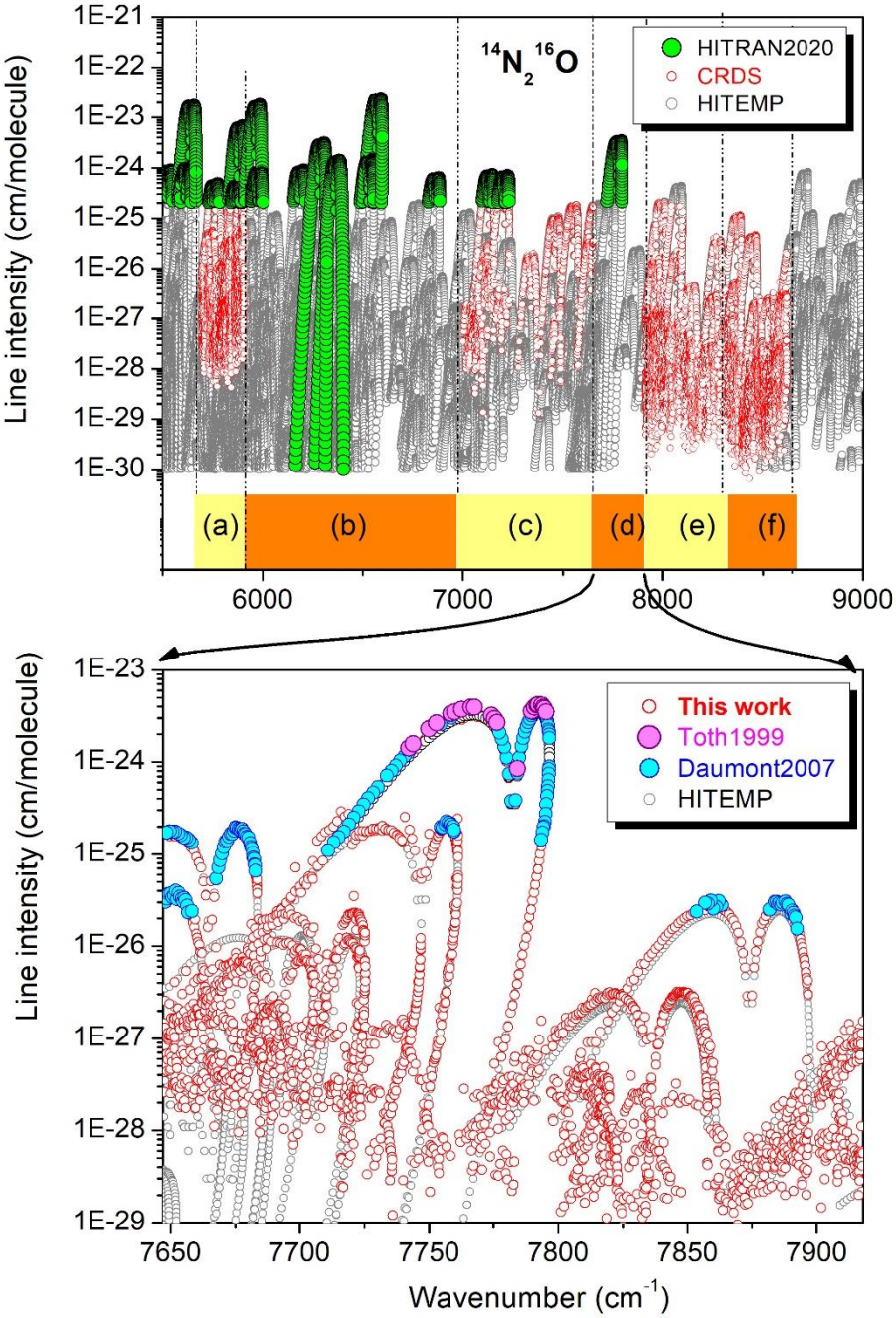

Fig. 1.

Overview of various line lists of $^{14}N_2{}^{16}O$ between 5500 and 9000 cm^{-1}

Upper panel: HITEMP and HITRAN2020 line lists (grey and green symbols, respectively). The range of previous CRDS investigations is indicated: (a): 5696- 5910 cm^{-1} [1], (b) 5905-7066 cm^{-1} [2-4], (c) 6950-7653 cm^{-1} [5,6], (d) 7647-7918 cm^{-1} [7], (e):7915-8334 cm^{-1} [8,9], (f): 8320-8622 cm^{-1} [10,11] and this work. Red circles correspond to CRDS intensities previously reported.

Lower panel: Enlargement of the (d) region corresponding to the range of the present study. FTS line lists of Refs. [15,16] (magenta and blue dots, respectively) and the present CRDS list (red circles) are superimposed to the HITEMP list [12] (grey).

2. Experimental details and line list construction

The description of the CRDS recordings is presented in Refs. [7,17] and not repeated here. Ten fibered distributed feed-back (DFB) diode lasers were used as light sources in order to cover continuously the 7647-7918 cm^{-1} region, except for an inaccessible gap between 7896.87 and 7901.17 cm^{-1}. Two series of spectra were recorded at a temperature of 293 K, for pressure values of 1 and 10 Torr. The 1 Torr spectra cover the low energy range (7647-7818.5 cm^{-1}) while the high energy region (7715-7918 cm^{-1}) corresponding to weaker absorption were recorded at 10 Torr. The typical value of the noise equivalent absorption coefficient was $\alpha_{min} \sim 1\times10^{-10}$ cm^{-1} (see Fig. 2 of Ref. [7]). The wavenumber scale of the spectra was calibrated with the help of a lambdameter and accurate reference line positions of H_2O (present as an impurity) taken from the HITRAN database [13]. Each spectral interval corresponding to the tuning range of one DFB laser diode (~20 cm^{-1}) was calibrated independently [7]. As indicated in Ref. [7], the maximum differences between line positions measured on the overlapping part of two successive spectra are less than of 2×10^{-3} cm^{-1} which leads to the 1×10^{-3} cm^{-1} average uncertainty value. Nevertheless, for the highest interval (7901-7918 cm^{-1}), the frequency calibration could not be checked in Ref. [7] by comparison with the nearby intervals. Here, by comparison with the line positions from Ref. [8] above 7915 cm^{-1}, we found that the frequency calibration of Ref. [7] for the 7901-7918 cm^{-1} interval has to be corrected by decreasing the wavenumber scale by 0.0025 cm^{-1} (this correction was validated by lower state combination relations performed during the band-by-band analysis).

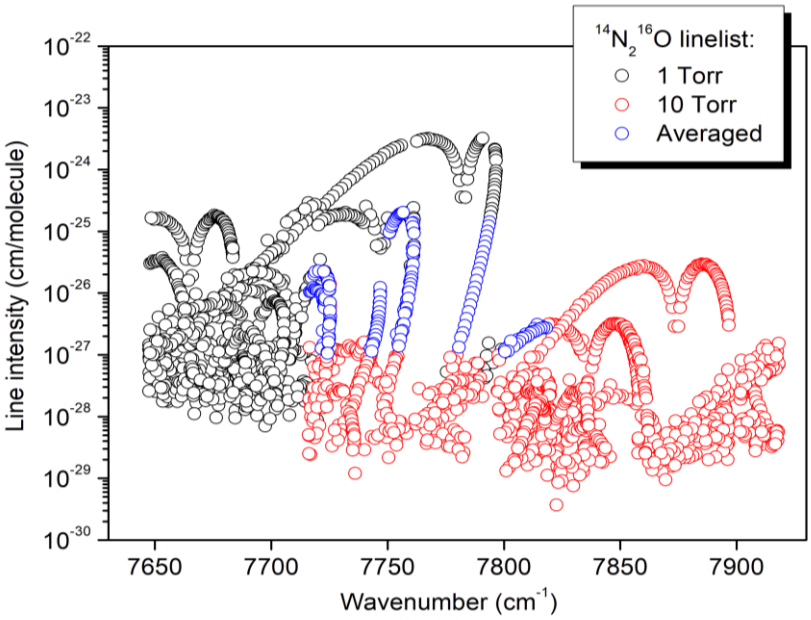

Fig. 2
Overview of the N_2O line list including the measurements at 1 and 10 Torr (black and red circles) and their averaged values (blue circles).

The line centers and intensities were determined using an interactive least squares multi-line fitting program assuming a Voigt function for the line profile The accuracy of the measured line intensities is about 3% or better for most lines and up to 20% for the weakest or strongly blended lines.

The complete line lists retrieved from the 1 Torr and 10 Torr spectra consist of 2185 and 2591 lines, respectively. In order to generate a single line list, in the overlapping part of the 1 and 10 Torr recordings (7715-7818.5 cm^{-1}), line parameters were averaged for the lines with intensity in the 10^{-27} - 2×10^{-25} cm/molecule range and for the weakest and strongest lines, the 10 Torr and 1 Torr line parameters were retained.

Overall, the global line list includes about 4100 entries. Lines due to water vapor, present as an impurity (73 and 38 lines at 1 and 10 Torr, respectively) were identified using the HITRAN line list [13] and removed from the list. The overview of the $^{14}N_2{}^{16}O$ line list obtained at the final stage of the assignment process (see below), is presented in **Fig. 2** with distinct colors according to the origin of the line parameters.

3. Rovibrational analysis

Overall, 3219 lines belonging to 49 bands of $^{14}N_2{}^{16}O$, $^{14}N^{15}N^{16}O$, $^{15}N^{14}N^{16}O$, $^{14}N_2{}^{18}O$, and $^{14}N_2{}^{17}O$ were identified. Except for four ΔP= 12 bands and two ΔP= 13 bands of the $^{14}N_2{}^{16}O$ isotopologue, all the bands belong to the ΔP= 14 series of transitions. **Fig. 3** compares the CRDS observations of the five N_2O isotopologues with the corresponding predictions of the respective effective operator models. The assignments were carried out based on the predictions of the global effective Hamiltonian models.

For $^{14}N_2{}^{16}O$, we used the non-polyad EH model [14]. In this model the eigenstates of the EH are not localized within a polyad. This means that all ΔP series of the transition intensities must be fitted with a single set of effective dipole moment parameters. This non-polyad EDM model is a generalization of the polyad EDM model which was used to fit the N_2O intensities so far (see e.g. [15]). The non-polyad EDM model of the line intensities will be presented in a separated publication. For other isotopologues, the polyad EH models [9,18] were used with a set of EH parameters refined using new line positions from Refs. [11,14,15,18]. For $^{14}N_2{}^{17}O$ line positions, we refitted data presented in Ref. [19] using measurements from Refs. [1,3,7,8].

In our region, all the observed bands of the minor isotopologues belong to the ΔP= 14 series of transitions. For each minor isotopologue, the corresponding EDM parameters were fitted to the measured intensities reported in [8] and then used to predict the line intensities.

Table 1
Comparison of the number of transitions and bands for the different N_2O isotopologues reported in Ref. [7] and obtained by CRDS in this work in the 7647–7918 cm^{-1} region.

Isotopologue	Abundance [13]	Number of transitions [a]	Number of bands [a]
$^{14}N_2{}^{16}O$	0.990333	2451(1746)	36(24)
$^{14}N^{15}N^{16}O$	3.64093×10^{-3}	151(89)	3(2)
$^{15}N^{14}N^{16}O$	3.64093×10^{-3}	291(167)	5(3)
$^{14}N_2{}^{18}O$	1.98582×10^{-3}	268(210)	4(3)
$^{14}N_2{}^{17}O$	3.69280×10^{-4}	58(60)	1(1)
Total		**3219(2272)**	**49(33)**

Note
[a] Numbers given within parentheses correspond to Ref. [7].

Table 1 compares the number of lines and bands identified in this work to our previous analysis of the same spectra in Ref. [7]. Compared to Ref. [7], 950 transitions are newly assigned and sixteen of the 49 bands are new (12, 1, 2 and 1 for $^{14}N_2{}^{16}O$, $^{14}N^{15}N^{16}O$, $^{15}N^{14}N^{16}O$, and $^{14}N_2{}^{18}O$, respectively). Note that the rotational structure of 23 of the bands identified extends below or above the studied 7647–7918 cm^{-1} region. In the following band-by-band analysis, the dataset of these bands will be complemented with measurements from Ref. [5] or Ref. [8] in the 6950-7653 cm^{-1} and 7915-

8334 cm^{-1} regions, respectively (see Fig. 1). Overall, twelve bands (8, 1, 2 and 1 for $^{14}N_2{}^{16}O$, $^{14}N^{15}N^{16}O$, $^{15}N^{14}N^{16}O$, and $^{14}N_2{}^{18}O$, respectively) and four sub-bands of $^{14}N_2{}^{16}O$ are newly measured. They are marked with "N" in Table 2.

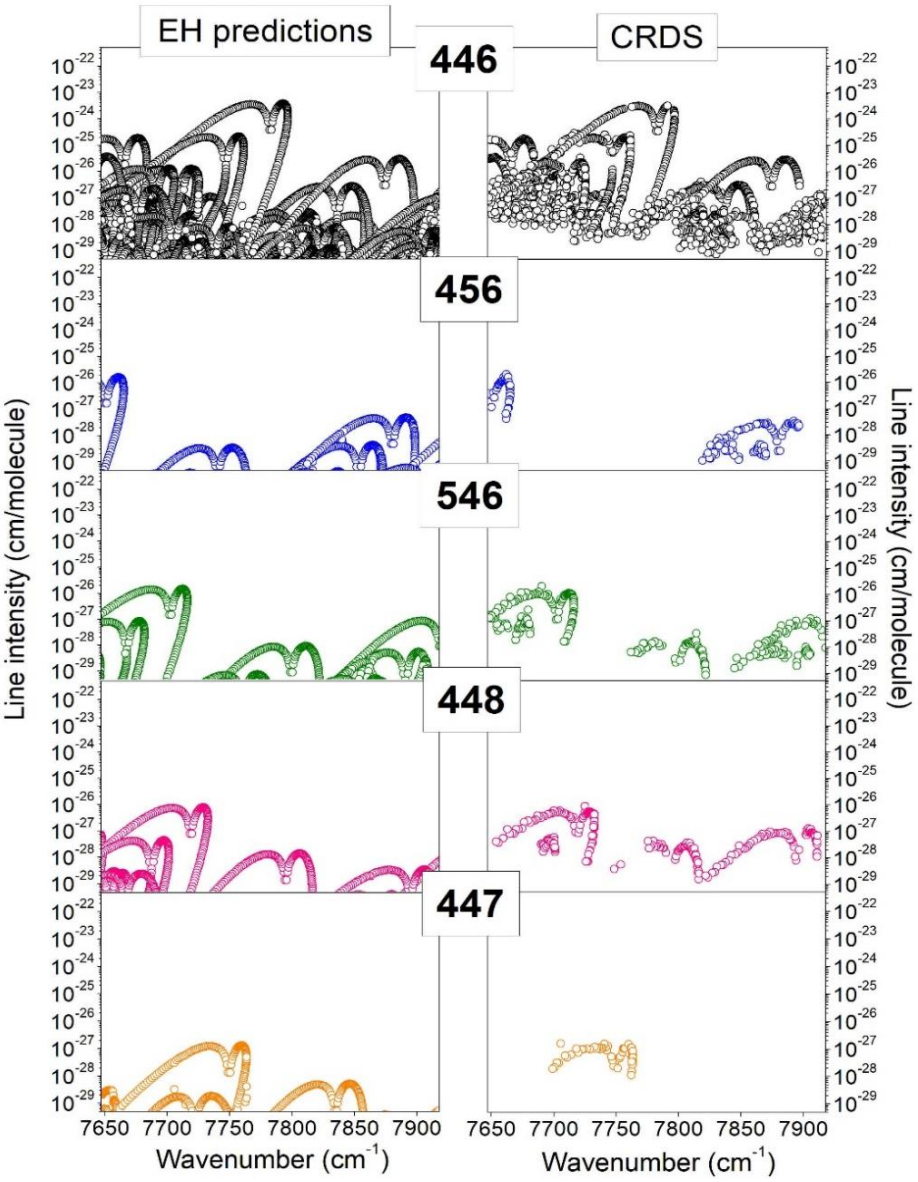

Fig. 3
Overview comparison between the transitions of $^{14}N_2{}^{16}O$ (446), $^{14}N^{15}N^{16}O$ (456), $^{15}N^{14}N^{16}O$ (546), $^{14}N_2{}^{18}O$ (448), and $^{14}N_2{}^{17}O$ (447) assigned between 7647 and 7918 cm^{-1} (right panels) and the corresponding spectra predicted in the frame of the effective operator approach (left panels).

The experimental line list, provided as Supplementary Material, includes the experimental and EH calculated positions and intensities for each line, together with corresponding rovibrational assignments and the measured line positions from Ref. [7] for comparison. Compared to Ref. [7], the transition dataset has been extended by about 950 new assignments and thus the fraction of unassigned lines is significantly reduced. About 230 and 570 lines at 1 and 10 Torr, respectively, are

left unassigned in the 7647-7918 cm^{-1} region. Most of them are very weak and not organized in regular series.

4. Band-by-band analysis

4.1. Band parameter fits

In the case of unperturbed bands, the rotational analysis was performed using the standard equation for the vibration–rotation energy levels:

$$F_v(J) = G_v + B_v J(J+1) - D_v J^2(J+1)^2 + H_v J^3(J+1)^3 \quad (1)$$

where G_v is the vibrational term value, B_v is the rotational constant, D_v and H_v are the centrifugal distortion constants, J is the angular momentum quantum number.

The spectroscopic parameters of the different upper states were fitted to the measured transition wavenumbers with lower state constants constrained to the values obtained by Toth [16,20]. Different sets of parameters were fitted for the *e* and *f* levels as the *e* and *f* sub bands may be perturbed in a different way (see below). In the case of upper states observed through different bands and branches, a global fit was performed in order to provide a unique set of parameters for each upper state. The detailed results of the band-by-band fit of the spectroscopic parameters are provided as Supplementary Material. Note that the rotational structure of 23 bands extend below or above the studied 7647–7918 cm^{-1} region under study. The line position dataset of these bands was complemented with measurements from Ref. [5] and Ref. [8] in the 6950-7653 cm^{-1} and 7915-8334 cm^{-1} regions, respectively (see **Fig. 1**). The added lines are tagged with their source in the fit results provided as Supplementary Material.

The retrieved constants of the upper states are listed in **Table 2**. The bands are ordered according to their band centers. Due to the reduced input data set (see Table 2 for details), for three very weak $^{14}N_2{}^{16}O$ hot bands, we give only the band center provided by the global effective Hamiltonian. The typical *rms* values of the fits are on the order of 1×10^{-3} cm^{-1}, which is consistent with our claimed accuracy on the line positions.

4.2. Local perturbations

Among the 49 analyzed bands, nine local perturbations were evidenced. The interaction mechanism, the perturber state and the *J* value of the angular momentum quantum number corresponding to the energy crossing was identified on the basis of the EH predictions (see **Table 3**).

Table 3

Local resonance interactions identified in the N_2O bands studied between 7647 and 7918 cm^{-1}

Isotopologue	Affected bands	Interacting states	J_{cross}	Interaction mechanism	Ref. [a]
$^{14}N_2{}^{16}O$	2003e-1000e 0802e-0200e	(16 0 7) ↔ (16 0 6)	32	Intrapolyad anharmonic	[7]
	2003e-0200e	(16 0 7) ↔ (16 0 6)	32	Intrapolyad anharmonic	TW
	1223e–0220e 1223f–0220f	(16 2 7) ↔ (15 1 13)	*e*: 32 *f*: 32	Interpolyad Coriolis	[7]
	3112e-0110e 3112f-0110f	(15 1 7) ↔ (15 1 8)	*e*: 46 *f*: 40	Intrapolyad anharmonic	[8]
	3202e-0200e	(16 0 10) ↔ (16 2 16) (16 0 10) ↔ (16 0 9)	26 49	Intrapolyad anharmonic + *l*-type Intrapolyad anharmonic	[8] TW
	3202e-1000e	(16 0 10) ↔ (16 2 16)	26	Intrapolyad anharmonic +*l*-type	TW
$^{14}N^{15}N^{16}O$	2202e-0000e	(14 0 8) ↔ (14 2 12)	34	Intrapolyad anharmonic + *l*-type	TW
$^{15}N^{14}N^{16}O$	3002e-0000e	(14 0 8) ↔ (14 2 11) (14 0 8) ↔ (14 0 6)	48 35	Intrapolyad anharmonic + *l*-type Intrapolyad anharmonic	[8] [8]
$^{14}N_2{}^{17}O$	1003-0000	(14 0 3) ↔(14 0 2)	70	Intrapolyad anharmonic	[7]

Note

[a] First report of the considered perturbation.

The (15 1 7) state (3112 in normal mode notation) is connected to the (15 1 8) state by an intrapolyad anharmonic interaction which induces an intensity transfer around the energy crossing at *J*= 46 and *J*= 40 for *e* and *f* sublevels, respectively. The 3112-0110 perturbed band is centered near 7970.4 cm^{-1}, thus above the spectral region under study. Most of the band was analyzed in Ref. [8] where the perturbation and the interaction mechanism were identified. Here, we observed part of the P-branch and we could newly identify 33 and 18 lines for *e* and *f* sublevels, respectively. A total of 9 extra lines could be assigned for the 3112e-0110e band around the *J* crossing value of 46, including some taken in the unassigned line list of Ref. [8]. The line parameters of these extra lines are included in the Supplementary Material. The residuals between the measured line positions of the 3112-0110 band and those calculated by using the spectroscopic constants of **Table 2** are presented in **Fig. 4.**

Similarly, most of the rotational structure of the perturbed 3202-0200 band centered near 7940.1cm^{-1} is located above our region and the perturbation was first evidenced in Ref. [8]. The 3202e upper state [(16 0 10) in cluster labelling notation] is in resonance anharmonic + *l*-type interaction with the (16 2 16) state around the energy crossing at *J* = 26. Due to intensity transfers, 6 extra lines around the crossing value *J*= 26 were identified in this work, one of them was assigned by using the unassigned line list of Ref. [8]. Also, another local perturbation affects the (16 0 10) state around *J*= 49. It is due to an intrapolyad anharmonic interaction with the (16 0 9) state. **Fig. 4** includes the plot of the deviations between the measured values of transition wavenumbers of the 3202e-0200e

band at 7940.2 cm^{-1} and the corresponding values calculated using the spectroscopic constants of **Table 2**.

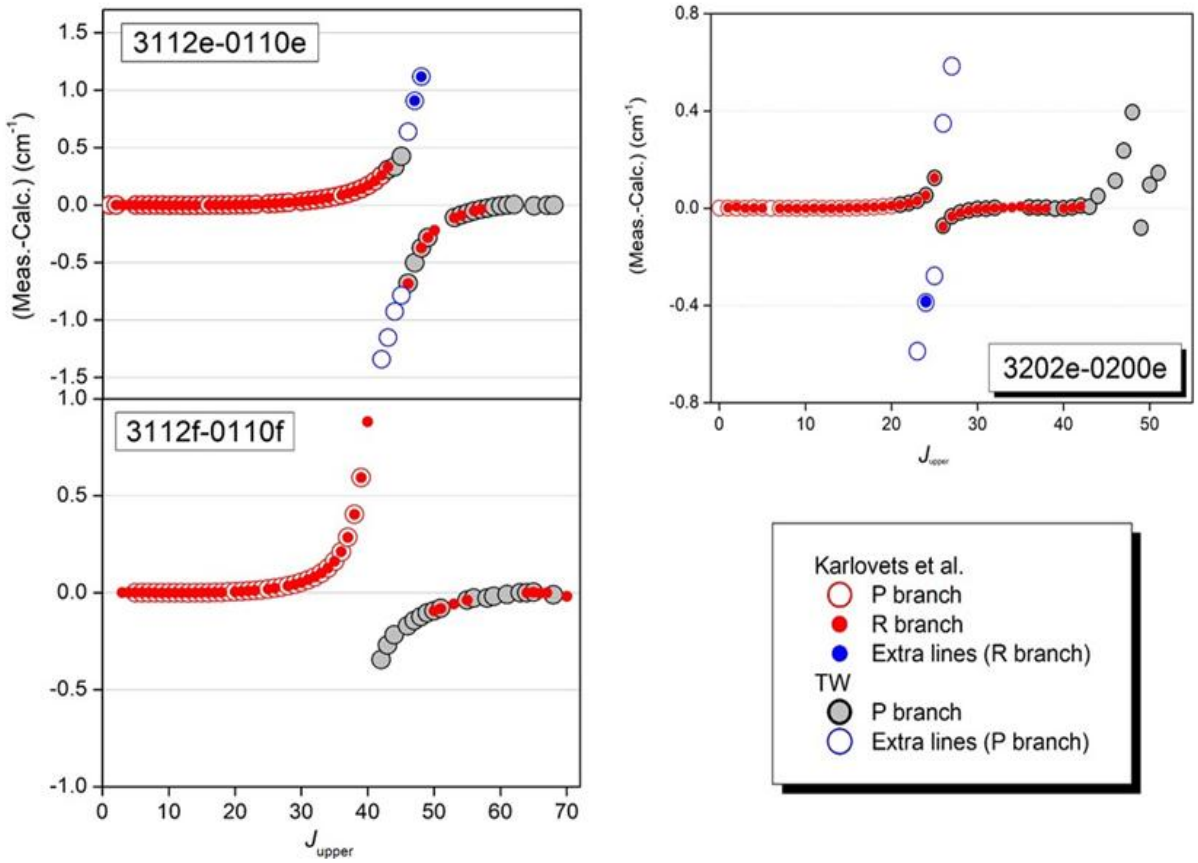

Fig. 4

Energy differences between the measured values and the values calculated using the spectroscopic parameters of Table 2, for the upper levels of two $^{14}N_2{}^{16}O$ bands affected by local perturbations. For each J_{upper} value, the values corresponding to the R(J_{upper} -1) (dots) and P(J_{upper} + 1) (open circles) are plotted. The two considered bands have their center located above the presently studied region (7647-7918 cm^{-1}) and only part of the P-branches was observed. The remaining part of the rotational structure was observed in Karlovets et al. [8] and is included in the plots.

Left panels

3112-0110 band at 7970.4 cm^{-1}. The (15 1 7) upper state is perturbed by an intrapolyad anharmonic interaction with the (15 1 8) state (energy crossing at *e:* J= 46; *f:* J= 40).

Right panel

3202e-0200e band at 7940.1 cm^{-1}. The (16 0 10) upper state is perturbed by an intrapolyad anharmonic +*l*-type interaction with the (16 2 16) state (energy crossing at J = 26) and by an intrapolyad anharmonic interaction with the (16 0 9) state (energy crossing at J = 49).

In the case of $^{14}N^{15}N^{16}O$ isotopologue, only the 2202e-0000e was found strongly perturbed. The interaction mechanism is presently identified as an intrapolyad anharmonic + *l*-type interaction between the (14 0 5) bright state and the (14 2 12) dark states with an energy crossing at J= 34. **Fig. 5** illustrates the effect of the resonance interaction. The perturbation induces a shift of the line positions up to 0.02 cm^{-1} around the energy crossing at J= 34.

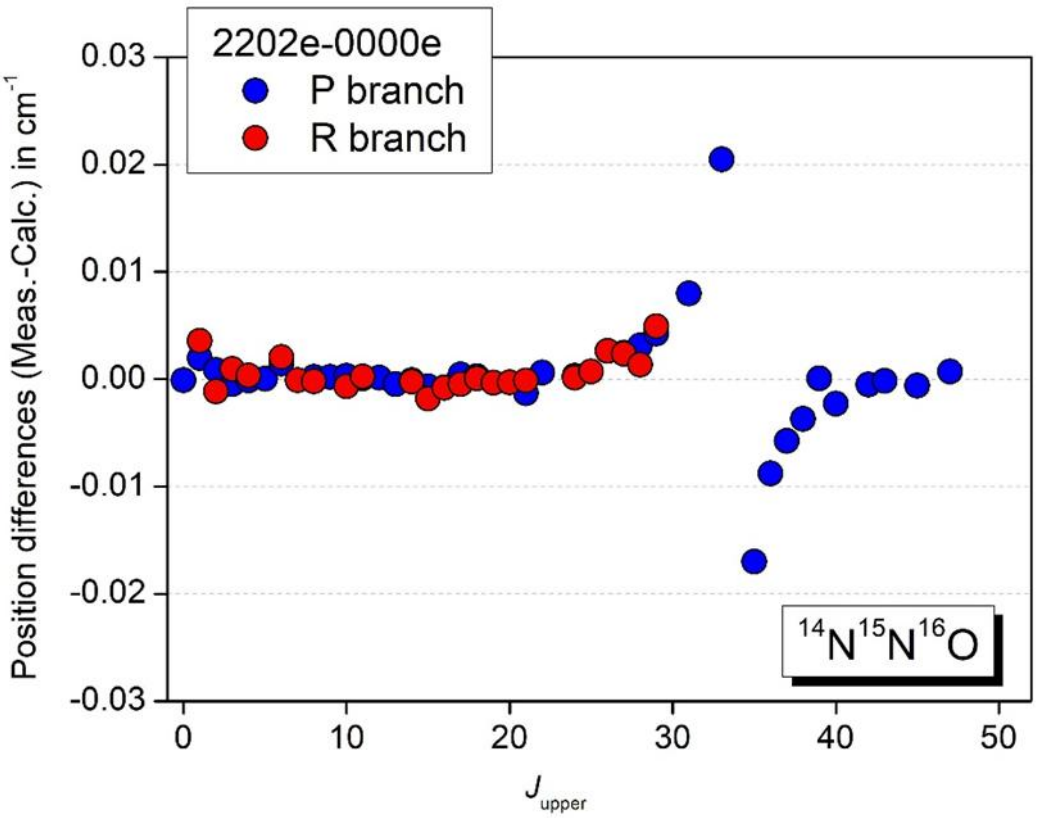

Fig. 5

Position differences between the measured line positions of the 2202e-0000e band ($^{14}N^{15}N^{16}O$) at 7880.386 cm^{-1} and the calculated ones using the spectroscopic parameters of Table 2. For each J_{upper} value, the values corresponding to the R(J_{upper} -1) (red circles) and P(J_{upper} + 1) (blue circles) are plotted. The (14 0 5) upper state is perturbed by an interpolyad anharmonic +/-type interaction with the (14 2 12) state (energy crossing at J = 34).

Several occurrences of intrapolyad interaction were already evidenced for the $^{15}N^{14}N^{16}O$ [8] and $^{14}N_2{}^{17}O$ [7] isotopologues. In particular, the upper state of the $\nu_1 + 3\nu_3$ band of $^{14}N_2{}^{17}O$ isotopologue is perturbed by an anharmonic interaction with the (14 0 2) state around the energy crossing at J = 70. The 3002e-0000e band of $^{15}N^{14}N^{16}O$ is perturbed by an anharmonic and an anharmonic +/-type interaction at J = 35 and J= 48, respectively.

5. Comparison with the calculated line lists

As detailed above, our assignments rely on improved predictions of the spectrum of the various N_2O isotopologues in the frame of the effective operator approach. Below, we first compare the observations to these (unpublished) predictions and then present the comparison to the available databases, namely HITRAN2020 [13], Nitrous Oxide Spectroscopy Databank (NOSD) [21] and HITEMP [12].

5.1. Present predictions

Fig. 6 and **Fig. 7** show an overview comparison between the observations and the predictions presently used for the spectrum analysis, for the line positions and line intensities, respectively. Overall, the agreement is satisfactory for line positions with deviations less than 0.02 cm^{-1} for the various isotopologues. This was expected as the line position measurements of Ref. [7] are part of the input data used to refine the used EH parameters. Nevertheless, significant differences are observed with deviation values depending on the vibrational bands. The largest disagreements, on the order of 0.04 cm^{-1}, are noted for the newly assigned 1113-0110 band of $^{14}N_2{}^{18}O$. For the main isotopologue, deviations with clear rotational dependence are noted for the 3820e-0220e band. This is probably related to the fact that the 3820e upper state is perturbed by an interpolyad Coriolis interaction with the 5510e state. The crossing point is around J= 26. The corresponding interaction term (ΔV_1= -2, ΔV_2= 3, Δl_2= 1, ΔV_3= 0) was accounted in our global fit *via* the main Coriolis parameter, only. The observed deviations indicate that the main term is not sufficient. In the next EH fits of $^{14}N_2{}^{16}O$ line positions, additional parameters will be added to better account for this Coriolis coupling.

The measured $^{14}N_2{}^{16}O$ line intensities are in reasonable agreement with the values predicted by the effective operator model (upper panel of **Fig. 7**) but important deviations are noted for some bands (note the logarithmic scale adopted for the ratios). As a rule, the deviations are due to underestimated calculated values due to some missing or inaccurate EDM parameters. For instance, the largest discrepancies (more than a factor 10) concern the 3311-0000 and 4111-0000 bands belonging to the ΔP= 13 series. These are the first ΔP= 13 bands observed with Δv_3= 1. Thus, the EDM parameters needed to model the intensities of such bands are unknown and the intensity values cannot be predicted accurately.

As concerns minor isotopologues (lower panel of **Fig. 7**), it is worth underlying that the experimental values should be taken with cautious as they rely on the (reasonable) assumption that the used sample has a natural isotopic abundance. Nevertheless, we can insure that, for a given isotopologue, the band-by-band change of the ratios is due to the calculations. For instance, the average ratios of the different $^{14}N_2{}^{18}O$ bands show large variations with a more than one order underestimation of the calculated intensity values for the 3002-0000 band. This band (as all those of the minor isotopologues in the region) belong to the ΔP= 14 series of transitions. The 3002-0000 band is a ΔP= 14 band with Δv_3= 2. There are two bands of this series (ΔP= 14 and Δv_3= 2) previously measured, namely the cold 2202e-0000e band [8] and the hot band 2312e/f-0110e/f [9]. The main EDM parameter M_{222} (see Ref. [23] for M parameter notation) responsible for the calculated intensities of this series was fitted to these measurements. In this work, the intensities of two other bands of this series were measured (3002e-0000e and 0602e-0000e). The EDM parameters which govern their

intensities, namely M_{302} and M_{060} were not previously determined leading to strong underestimations of the predicted intensities.

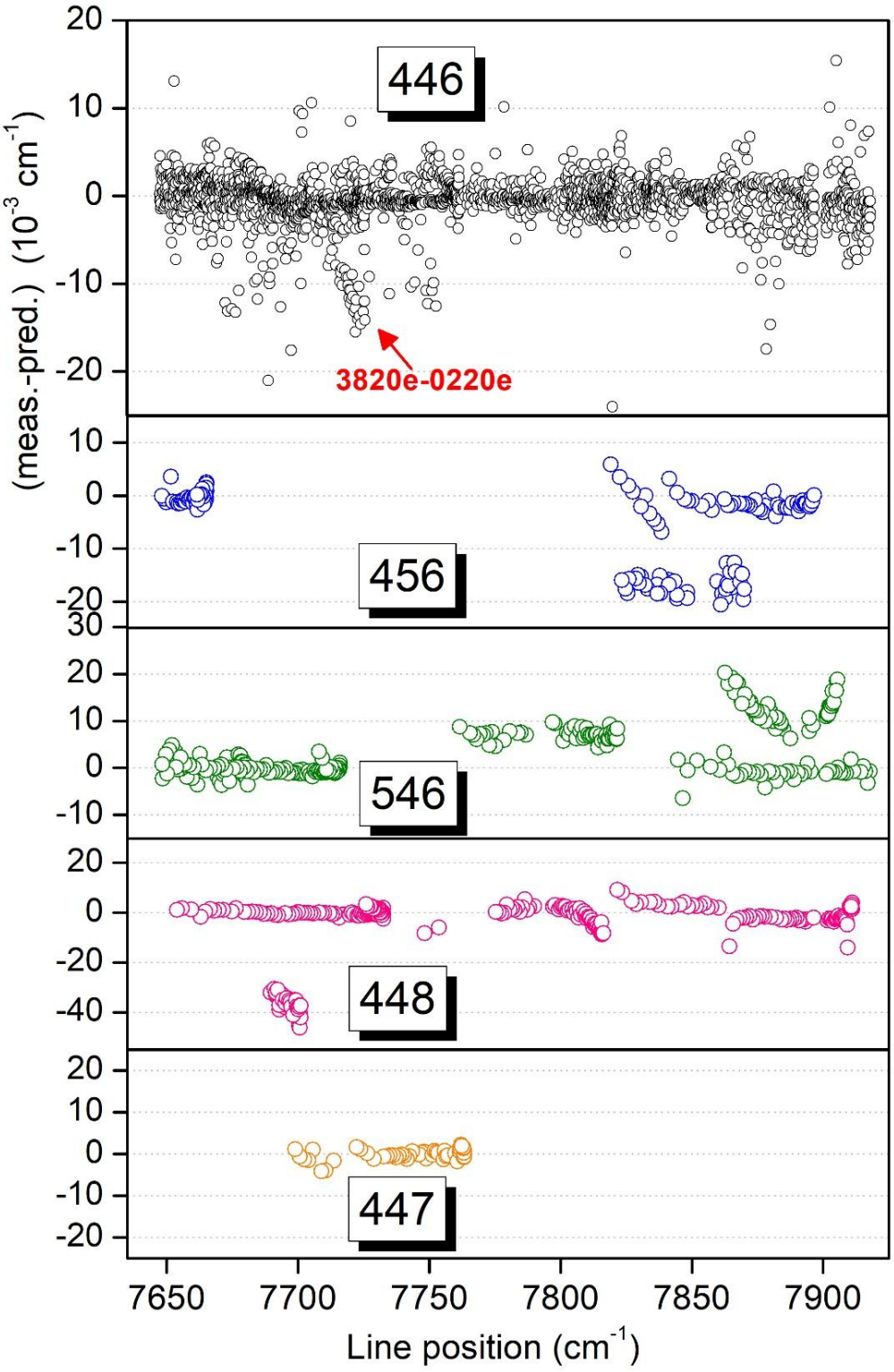

Fig. 6

Position differences between the measured and predicted values for the various N_2O isotopologues contributing to the spectrum in the 7647 - 7918 cm^{-1} spectral region.

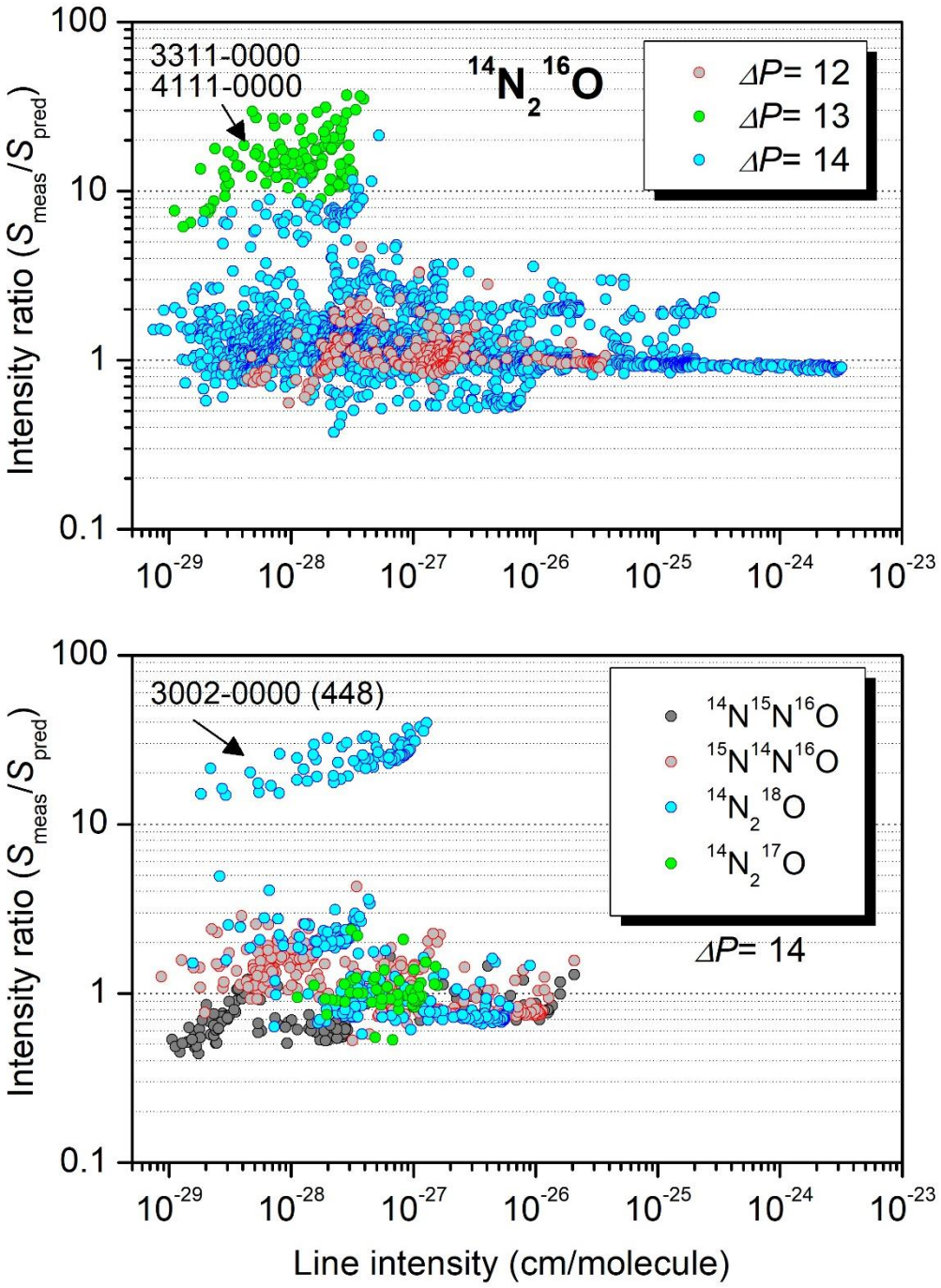

Fig. 7

Intensity ratios of the measured N_2O line intensities to those predicted by EDM the effective operator model in the 7647 - 7918 cm^{-1} spectral region. Note the logarithmic scale adopted for the ordinate scale.

Upper panel: Main isotopologue, $^{14}N_2{}^{16}O$. The values corresponding to ΔP = 12, 13 and 14 are plotted with different colors,

Lower panel: Minor isotopologues: $^{14}N^{15}N^{16}O$, $^{15}N^{14}N^{16}O$, $^{14}N_2{}^{18}O$, and $^{14}N_2{}^{17}O$. All transitions belong to the ΔP = 14 band series.

5.2. HITRAN2020, NOSD-1000 and HITEMP

As illustrated in **Fig. 1**, the HITRAN2020 line list [13] is limited to the 90 strongest transitions of the $\nu_1+3\nu_3$ band of the main isotopologue. The source of the HITRAN line parameters in our region is the database constructed by Toth from FTS spectra (although the HITRAN database gives as source "R.A. Toth, Jet Propulsion Laboratory, Linelist of N_2O parameters from 500 to 7500 cm^{-1}, private communication" which is outside our region…).

The NOSD-1000 line list of $^{14}N_2{}^{16}O$ is a high temperature line list calculated in 2016 within the effective operator approach [21]. Its intensity cutoff is 10^{-25} cm/molecule at 1000 K. The HITEMP N_2O line list [12] was constructed in 2019 by merging three NOSD line lists at 296, 500 and 1000 K (of $^{14}N_2{}^{16}O$) in order to make the list applicable over the 296-1000 K range (it thus includes the NOSD-1000 list). The HITEMP list reproduces HITRAN for the minor isotopologues.

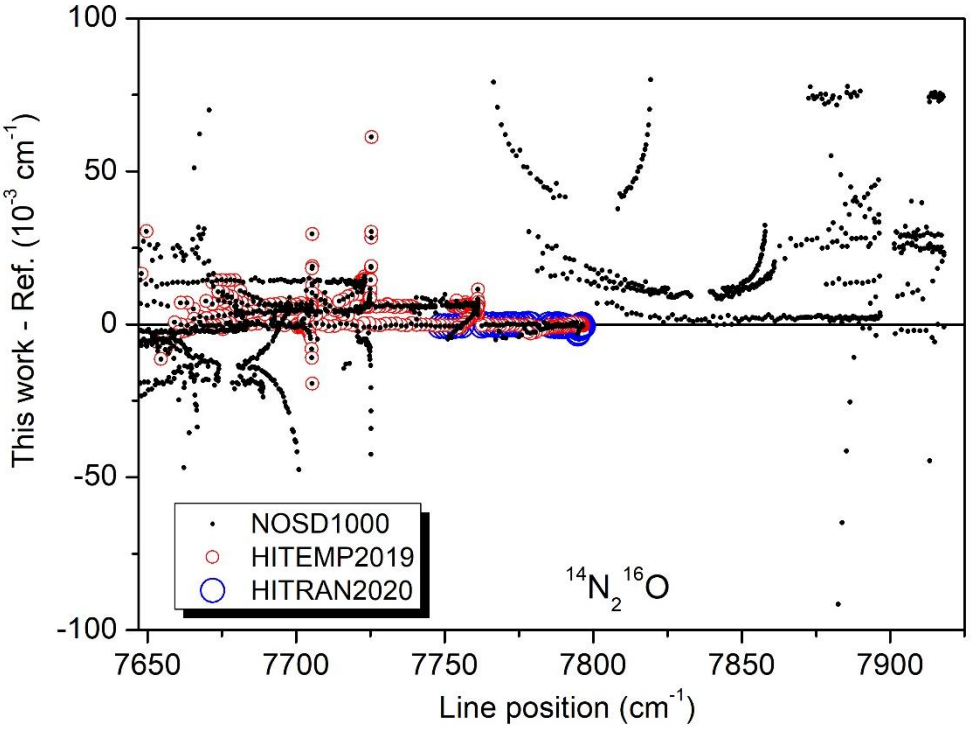

Fig. 8

Differences between the measured position values of $^{14}N_2{}^{16}O$ and the corresponding values provided by the HITRAN2020 [13], NOSD-1000 [21] and HITEMP [12] spectroscopic databases (blue open circles, red open circles and black dots, respectively), in the 7647 - 7918 cm^{-1} spectral region.

Fig. 8 and **Fig. 9** show an overview comparison between the observations and the various databases for positions and intensities, respectively. As expected, the literature databases (all calculated) show more important deviations from the measurements than the refined calculated line lists used for the above assignments. Roughly, a gain by one order of magnitude has been achieved on the position values compared to HITEMP2019. As for line intensities, deviations are similar to those of the present predictions, with significant underestimation of HITEMP intensities for a number of

bands. Note that the 3311-0000 and 4111-0000 bands belonging to the ΔP= 13 series which show the largest deviations compared to the present predictions are absent in the HITEMP database.

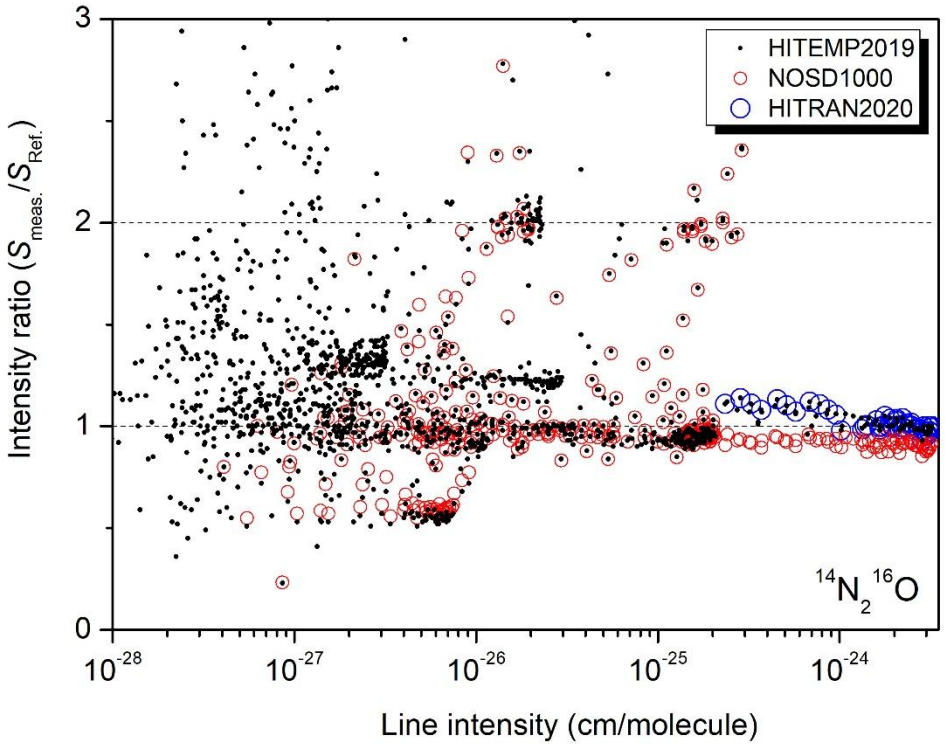

Fig. 9

Intensity ratios of the measured $^{14}N_2{}^{16}O$ line intensities to the predicted values provided by the HITRAN2020 [13], NOSD-1000 [21] and HITEMP [12] spectroscopic databases (blue open circles, red open circles and black dots, respectively), in the 7647 - 7918 cm^{-1} spectral region.

6. Conclusion

The characterization of the absorption spectrum of nitrous oxide has been significantly improved between 7647 and 7918 cm^{-1} by *(i)* the systematic retrieval of the line intensities, *(ii)* the extension of the rovibrational assignments (about 950 assignments added to the 2272 previously reported from the same spectra in Ref. [7]), *(iii)* the detailed analysis of a number of local rovibrational perturbations.

The reported observations will help to improve the N_2O line lists in the spectroscopic databases in terms of completeness and accuracy. In particular, in the considered region, the HITRAN list includes only about 90 transitions of the ν_1+3ν_3 band for the main isotopologue while 2451 transitions of 36 bands have been identified in the present work. As concerns the NOSD-1000 [21] and HITEMP [12] line lists calculated in the frame of the effective operator approach, part of the positions and intensities deviate significantly from the observations. This is due to the lack of previous experimental data which prevented the determination of some relevant EH or EDM parameters.

Due to the existence of interpolyad couplings in N_2O, a non-polyad effective Hamiltonian model has been recently elaborated for $^{14}N_2{}^{16}O$ [14]. For consistency, a non-polyad effective dipole moment model is under construction. A single set of effective dipole moment parameters for all ΔP series will be determined from a global fit of the transition intensities available in the literature. In this context, together with previous sets of line intensities measured by CRDS (see **Fig. 1**), the intensity information obtained in this work will bring strong constraints to the non-polyad EDM parameters. Let us mention that in the future, intensity information will be completed from a systematic intensity retrieval from the CRDS spectra in the5905-7647 cm^{-1} region [intervals (b) and (c) in **Fig. 1**].

Acknowledgements

This work was performed during the stay of the first author in Grenoble supported by a Metchnikov grant from the French Embassy in Russia. SAT acknowledges the support of the Ministry of Science and Higher Education of the Russian Federation. This project is supported by CNRS (France) in the frame of the International Research Project "SAMIA".We acknowledge the GRICAD cluster infrastructure of the University Grenoble Alpes (https://gricad.univ-grenoble-alpes.fr): the DAHU cluster was used for some computations performed in in the framework of the n2oandco2 research project.

References

1. Bertin T, Mondelain D, Karlovets EV, Kassi S, Perevalov VI, Campargue A. High sensitivity cavity ring down spectroscopy of N_2O near 1.74 μm. J Quant Spectrosc Radiat Transf 2019;229:40–9. doi: 10.1016/j.jqsrt.2019.02.011.
2. Liu AW, Kassi S, Perevalov VI, Tashkun SA, Campargue A. High sensitivity CW-cavity ring down spectroscopy of N_2O near 1.5 μm (II). J Mol Spectrosc 2007:244;48-62. doi: 10.1016/j.jms.2007.05.010.
3. Liu AW, Kassi S, Malara P, Romanini D, Perevalov VI, Tashkun SA, Hu SM, Campargue A. High sensitivity CW-cavity ring down spectroscopy of N_2O near 1.5 μm (I). J Mol Spectrosc 2007:244;33-47. doi: 10.1016/j.jms.2006.03.007.
4. Liu AW, Kassi S, Perevalov VI, Hu SM, Campargue A. High sensitivity CW-cavity ring down spectroscopy of N_2O near 1.5 μm (III). J Mol Spectrosc 2009;254:20–7. doi: 10.1016/j.jqsrt.2019.02.011.
5. Lu Y, Mondelain D, Liu AW, Perevalov VI, Kassi S, Campargue A. High Sensitivity *CW*-Cavity Ring Down Spectroscopy of N_2O between 6950 and 7653 cm^{-1} (1.44-1.31 μm): I. Line positions. J Quant Spectrosc Radiat Transfer 2012;113:749-62. doi: 10.1016/j.jqsrt.2012.03.005.
6. Karlovets EV, Lu Y, Mondelain D, Kassi S, Campargue, Tashkun SA, Perevalov VI, High sensitivity CW-Cavity Ring Down Spectroscopy of N_2O between 6950 and 7653 cm^{-1} (1.44–1.31 μm): II. Line intensities. J Quant Spectrosc Radiat Transfer 2013;117:81–7. doi: 10.1016/j.jqsrt.2012.11.003.
7. Liu AW, Kassi S, Perevalov VI, Tashkun SA, Campargue A. High sensitivity CW-cavity ring down spectroscopy of N_2O near 1.28 μm. J Mol Spectrosc 2011:267;191-9. doi:10.1016/j.jms.2011.03.025.
8. Karlovets EV, Campargue A, Kassi S, Perevalov VI, Tashkun SA. High sensitivity Cavity Ring Down Spectroscopy of N_2O near 1.22 μm: (I) Rovibrational assignments and band-by-band analysis. J Quant Spectrosc Radiat Transfer 2016;169:36–48. doi: 10.1016/j.jqsrt.2019.02.011.
9. Tashkun SA, Perevalov VI, Karlovets EV, Kassi S, Campargue A. High sensitivity Cavity Ring Down Spectroscopy of N_2O near 1.22 μm: (II) $^{14}N_2{}^{16}O$ line intensity modeling and global fit of $^{14}N_2{}^{18}O$ line positions. J Quant Spectrosc Radiat Transfer 2016;176:62–69. doi: 10.1016/j.jqsrt.2016.02.020.
10. Karlovets EV, Kassi S, Tashkun SA, Campargue A. The absorption spectrum of nitrous oxide between 8325 and 8622 cm^{-1} J Quant Spectrosc Radiat Transf 2021;262:107508. doi: 10.1016/j.jqsrt.2021.107508.
11. Karlovets EV, Tashkun SA, Kassi S, Campargue A. An improved analysis of the N_2O absorption spectrum in the 1.18 μm window. J Quant Spectrosc Radiat Transf 2022;278:108003. doi: 10.1016/j.jqsrt.2021.108003.
12. Hargreaves RJ, Gordon IE, Rothman LS, Tashkun SA, Perevalov VI, Lukashevskaya AA, et al. Spectroscopic line parameters of NO, NO_2, and N_2O for the HITEMP database. J Quant Spectrosc Radiat Transfer 2019;232:35–53. doi:10.1016/j.jqsrt.2019.04.040.
13. Gordon IE, Rothman LS, Hargreaves RJ, Hashemi R, Karlovets EV, Skinner FM, Conway EK, et al. The HITRAN2020 molecular spectroscopic database. J Quant Spectrosc Radiat Transf, 2022;277:107949. doi: 10.1016/j.jqsrt.2021.107949.
14. Tashkun SA. Global modeling of the $^{14}N_2{}^{16}O$ line positions within the framework of the nonpolyad model of effective Hamiltonian. J Quant Spectrosc Radiat Transf 2019;231:88–101, doi: 10.1016/j.jqsrt.2019.04.023.
15. Daumont L, Van der Auwera J, Teffo JL, Perevalov VI, Tashkun SA. Line intensity measurements in $^{14}N_2{}^{16}O$ and their treatment using the effective dipole moment approach. II. The 5400-11000 cm^{-1} region. J Quant Spectrosc Radiat Transfer 2007;104:342–56. doi: 10.1016/j.jqsrt.20 06.09.004.
16. Toth RA. Line positions and strengths of N_2O between 3515 and 7800 cm^{-1}. J Mol Spectrosc 1999;197:158–87. doi: 10.1006/jmsp.1999.7907.

17. Macko P, Romanini D, Mikhailenko SN, Naumenko OV, Kassi S, Jenouvrier A, Tyuterev VG, Campargue A. High sensitivity CW-cavity ring down spectroscopy of water in the region of the 1.5 μm atmospheric window. J Mol Spectrosc 2004;227(1):90–108. doi: 10.1016/j.jms.2004.05.020.
18. Tashkun SA, Perevalov VI, Kochanov RV, Liu AW, Hu SM. Global fitting of $^{14}N^{15}N^{16}O$ and $^{15}N^{14}N^{16}O$ vibrational-rotational line positions using the effective Hamiltonian approach. J Quant Spectrosc Radiat Transf 2010;111(9):1089–105. doi: 10.1016/j.jqsrt.2010.01.010.
19. Vlasova AV, Perevalov BV, Tashkun SA, Perevalov VI. Global fittings of the line positions of the rare isotopic species of the nitrous oxide molecule, Proc. of SPIE Vol. 2006;6580:658007.
20. Toth RA. Linelist of N_2O parameters from 500 to 7500 cm^{-1}. http://mark4sun.jpl.nasa.gov/n2o.html
21. Tashkun SA, Perevalov VI, Lavrentieva NN. NOSD-1000, the high-temperature nitrous oxide spectroscopic databank. J Quant Spectrosc Radiat Transfer 2016;177:43–8. https://doi.org/10.1016/j.jqsrt.2015.11.014.
22. Gordon IE, Rothman LS, Hill C, Kochanov RV, Tan Y, Bernath PF, et al. The HITRAN2016 molecular spectroscopic database. J Quant Spectrosc Radiat Transf 2017;203:3–69. doi: 10.1016/j.jqsrt.2017.06.038 .
23. Lyulin OM, Perevalov VI, Teffo JL, Effective Dipole Moment and Band Intensities of Nitrous Oxide, J. Mol. Spectrosc. 1995;174:566–80. https://doi.org/10.1006/jmsp.1995.0023)

Table 2. Spectroscopic parameters (in cm^{-1}) for the different bands of N_2O isotopologues assigned in the CRDS spectrum between 7647 and 7918 cm^{-1}.

Band[a]	$(P\ l_2\ i)$[b]	ΔG_v[c]	G_v	B_v	$D_v \times 10^7$	$H_v \times 10^{12}$	RMS[d]	N_{fit}/N_{obs}[e]	$J_{max\ P/Q/R}$[f]	ΔP[g]	Note[h]
$^{14}N_2{}^{16}O$											
3600e-0000e 4400e-0000e[k]	(12 0 16)	7640.47399(11)	7640.47399(11)	0.41184936(35)	-8.50(28)	8.782(61)	0.49	137/147	P57/R57	12	1
2113e-1110e	(17 1 7)	7657.000257(60)	9537.26849(60)	0.4055439(43)	0.423(52)		0.94	12/21	P17/R27	14	1
2113f-1110f		7657.00026(80)	9537.26832(80)	0.406515(20)	-9.6(10)		0.84	11/16	P14/R23	14	1
1004e-0001e	(18 0 4)	7664.81052(47)	9888.56729(47)	0.4033368(29)	1.629(35)		0.88	22/27	P29/R28	14	1
0203e-0000e	(14 0 1)	7665.273385(68)	7665.273385(68)	0.40978312(18)	2.5006(10)	3.320(16)	0.49	197/200	P72/R63	14	1
0223e-0000e	(14 2 1)	7673.63782(50)	7673.63783(50)	0.4099796(10)	1.1509(58)	-3.593(92)	0.71	66/85	P65/R52	14	1
1333e-0330e	(17 3 3)	7674.09763(15)	9441.01001(15)	0.40909338(39)	1.5836(19)		0.68	80/90	P50/R44	14	1
1333f-0330f N		7674.09828(30)	9441.01052(30)	0.40909061(96)	1.5424(57)		0.75	23/25	P24/R41	14	
1333f-0330e N								3/5	Q11	14	
3710e-0110e	(13 1 16)	7677.51591(14)	8266.28378(14)	0.41080395(68)	0.9997(80)	5.79(24)	0.59	101/117	P52/R41	12	1
3710e-0110f N								1/2	Q02	12	
3710f-0110f		7677.51574(14)	8266.28361(14)	0.41338803(60)	0.3976(61)	3.70(16)	0.68	121/130	P54/R44	12	1
1512e-0110e N	(15 1 2)	7678.870122[l]	8268.46690[m]					/9	P24/R36	14	
1512f-0110f N		7678.870106[l]	8268.47233[m]					/14	P27/R29	14	
2003e-1000e	(16 0 7)	7691.58483(11)	8976.48817(11)	0.40513544(55)	1.6707(45)	2.39(10)	0.73	40/60	P30/R48	14	2
2003e-0200e	(16 0 7)	7808.35587(11)						96/168	P59/R51	14	1,3
3820e-0220e N	(14 2 16)	7705.61362(63)	8883.35829(63)	0.4124361(32)	2.694(34)	-	0.80	19/24	P33/R29	12	
3820f-0220f N		7705.61272(50)	8883.35739(50)	0.4124294(25)	0.889(25)	-	0.60	15/20	P31/R30	12	
1203e-0200e	(16 0 4)	7708.908827(93)	8877.041127(93)	0.40796933(32)	2.4131(24)	2.896(50)	0.59	172/181	P62/R56	14	1
1223e-0220e	(16 2 3)	7710.77475(99)	8888.51942 (99)	0.40837821(48)	1.2625(32)	-1.759(57)	0.55	79/167	P48/R62	14	1,4
1223e-0220f N								11/15	Q20	14	
1223f-0220f		7710.77505(13)	8888.51972(13)	0.40837451(60)	1.8035(49)	2.51(11)	0.66	103/174	P57/R54	14	1,4
1223f-0220e N								4/5	Q17	14	
4111e-0000e	(13 1 10)	7715.06542(45)	7715.06542(45)	0.41075365(92)	1.9302(36)		0.67	20/26	P13/R48	13	
4111f-0000e		7715.06296(63)	7715.06296(63)	0.4125991(27)	1.959(21)		0.67	11/15	Q34	13	
0602e-0000e 3002e-0000e[k]	(14 0 2)	7722.58736(17)	7722.58736(17)	0.41474349(83)	6.2695(97)	46.13(29)	0.57	58/68	P41/R48	14	
4600e-0200e N	(14 0 20)	7738.47827(78)	8906.61057(78)	0.4113308(77)	-0.83(15)		0.89	11/14	P22/R21	12	
1113e-0110e	(15 1 3)	7747.02854(84)	8335.796410(84)	0.40719799(23)	1.7159(14)	0.122(23)	0.48	176/198	P67/R67	14	1
1113e-0110f								26/31	Q40	14	

1113f-0110f		7747.028142(81)	8335.796012(81)	0.40804222(20)	1.7030(11)	0.339(16)	0.48	177/198	P70/R68	14	1
1113f-0110e								34/35	Q40	14	
0912e-0310e N	(17 1 10)	7765.798975[l]	9661.79043[m]					/21	P37	14	
0912f-0310f N		7765.799826[l]	9661.79502[m]					/13	P28	14	
1003e-0000e	(14 0 3)	7782.661469(83)	7782.661469(83)	0.40682441(14)	1.7052(56)	0.1833(61)	0.43	124/128	P75/R82	14	
0822e-0220e	(16 2 5)	7799.82850(25)	8977.57317(25)	0.4130224(10)	- 1.064(98)	-35.08(25)	0.66	55/60	P40/R51	14	
0822f-0220f		7799.82956(20)	8977.57423(20)	0.41302649(83)	2.5672(86)	2.59(23)	0.56	56/59	P40/R50	14	
0802e-0200e 0802e-0000e[k]	(16 0 6)	7800.70549(27)	8968.83779(27)	0.4128192(12)	5.577(11)	30.28(29)	0.73	40/69	P41/R52	14	2
3311e-0000e 3310e-0000e[k]	(13 1 12)	7817.83164(20)	7817.83164(20)	0.40971292(74)	1.2793(45)		0.68	39/49	P17/R42	13	
3311f-0000e		7817.83240(30)	7817.83240(30)	0.4113001(11)	0.9355(74)		0.68	32/36	Q41	13	
0712e-0110e 2312e–0110e[k]	(15 1 5)	7836.25583(15)	8425.02371(15)	0.41147721(61)	2.5344(53)	3.75(12)	0.75	91/97	P55/R57	14	
0712e-0110f N								15/19	Q27	14	
0712f-0110f 2312f–0110f[k]		7836.25541(13)	8425.02328(13)	0.41365611(27)	2.7122(10)		0.71	86/93	P45/R56	14	
0712f-0110e N								12/13	Q25	14	
1403e-0001e N	(18 0 8)	7855.8086(11)	10079.5654(11)	0.4060705(45)	2.129(39)		0.83	11/20	P30/R31	14	
2202e-0000e	(14 0 5)	7874.15546(12)	7874.15546(12)	0.41216104(40)	3.7169(29)	11.964(50)	0.58	96/107	P60/R66	14	
0622e-0000e 2220e-0000e[k]	(14 2 4)	7884.02171(44)	7884.02171(44)	0.4124230(10)	0.3705(64)	-12.22(11)	0.63	51/65	P61/R58	14	
4112e-1110e N	(17 1 11)	7903.51036(44)	9783.77610(44)	0.4074211(17)	1.996 (13)		0.81	30/35	P36/R24	14	
4112f-1110f N		7903.50935(58)	9783.77509(44)	0.4091909(19)	2.014(17)		0.67	21/31	P34/R22	14	
3312e-0310e	(17 1 10)	7911.90362(27)	9660.96885(27)	0.4094902(14)	1.977(12)		0.72	28/31	P08/R33	14	5
3312f-0310f		7911.90528(38)	9660.97044(38)	0.4117341(31)	1.137(20)		0.80	7/37	P07/R05	14	5
0912e-0310e N	(17 1 6)	7911.906629[l]	9515.68961[m]					/18	P37	14	
0912f-0310f N		7911.905789[l]	9515.69535[m]					/9	P28	14	
3332f-0330f	(17 3 8)	7916.99502(24)	9683.90739(24)	0.4113731(15)	1.728(21)	11.35(21)	0.63	31/34	P33/R44	14	5
3332f-0330e								6/6	Q11	14	5
4002e-1000e	(16 0 11)	7934.15251(18)	9219.05585(18)	0.40751321(64)	2.3439(51)	2.40(11)	0.73	79/93	P54/R60	14	5
3222e-0220e	(16 2 8)	7943.49717(19)	9121.24184(19)	0.41072577(84)	0.5451(68)		0.71	50/62	P36/R37	14	5
3222f-0220f		7943.49759(27)	9121.24226(27)	0.4107322(15)	2.041(22)	9.27(91)	0.59	34/34	P36/R40	14	5
3222f-0220e								7/8	Q11	14	5
3112e-0110e	(15 1 8)	7970.41297(18)	8559.18084(18)	0.4093019(11)	2.4733(60)	7.420(93)	0.71	37/113	P69/R56	14	5,6

3112e-0110f								14/15	Q19	14	5
3112f-0110f		7970.41314(17)	8559.18101(17)	0.4109471(13)	2.4786(68)	5.71(11)	0.58	33/94	P65/R66	14	5,6
3112f-0110e								10/13	Q18	14	5
3002e-0000e	(14 0 8)	7998.6264(62)	7998.6264(62)	0.4094239(29)	2.1128(32)		0.90	15/20	P78	14	5
3202e-0200e	(16 0 10)	7940.09975(21)	9108.32305(21)	0.4103225(21)	4.447(32)	85.6(13)	0.78	36/95	P52/R41	14	5,7,8
3202e-1000e	(16 0 10)	7823.41971(21)						16/42	P25/R33	14	9
$^{14}N^{15}N^{16}O$											
1003e-0000e	(14 0 3)	7650.753893(96)	7650.753893(96)	0.40710138(21)	1.73037(77)		0.60	127/142	P58/R54	14	1
1512e-0110e N	(15 1 5)	7853.58564(74)	8429.01929(74)	0.4094226(51)	2.140(72)		0.87	18/23	P26/R25	14	
1512f-0110f N		7853.58373(70)	8429.01738(70)	0.4111180(41)	2.207(47)		0.79	17/23	P28/R27	14	
2202e-0000e	(14 0 8)	7880.38631(18)	7880.38631(18)	0.4097635(11)	2.829(14)	13.31(49)	0.59	42/61	P48/R28	14	10
$^{15}N^{14}N^{16}O$											
1113e-0110e	(15 1 3)	7667.80653(31)	8253.11865(31)	0.39349566(98)	1.5853(54)		0.78	40/58	P44/R27	14	1
1113f-0110f		7667.80403(26)	8253.11615(26)	0.3943259(12)	1.946(11)		0.88	48/63	P36/R25	14	1
1003e-0000e	(14 0 3)	7702.499365(77)	7702.499365(77)	0.39310842(28)	1.5827(22)	0.444(45)	0.51	169/177	P62/R59	14	1
2202e-0000e N	(14 0 5)	7799.40281(30)	7799.40281(30)	0.3981881(14)	3.152(17)	7.41(53)	0.74	45/53	P36/R46	14	
3112e-0110e N	(15 1 8)	7890.93194(63)	8476.24406(63)	0.3956738(88)	3.71(30)		0.76	25/28	P27/R25	14	
3112f-0110f N		7890.93088(80)	8476.24300(80)	0.397278(12)	6.75(50)		0.76	19/23	P24/R22	14	
3002e-0000e	(14 0 8)	7918.58234(32)	7918.58234(32)	0.3957901(22)	2.635(14)	8.73(25)	0.83	32/124	P56/R58	14	1,5,11
$^{14}N_2{}^{18}O$											
1113e-0110e N	(15 1 3)	7687.32065(48)	8271.54531(48)	0.3847327(27)	1.435(26)		0.71	13/21	R30	14	
1113f-0110f N		7687.32155(63)	8271.54621(63)	0.3855560(34)	1.282(36)		0.78	13/17	R29	14	
1003e-0000e	(14 0 3)	7718.947472(91)	7718.947472(91)	0.38434145(32)	1.4612(26)	0.599(55)	0.54	176/185	P57/R58	14	1
0602e-0000e 1402e-0000e [k]	(14 0 2)	7794.88604(20)	7794.88604(20)	0.38874088(95)	2.8185(96)	5.82(26)	0.62	52/57	P43/R50	14	
3002e-0000e	(14 0 8)	7894.89002(17)	7894.89002(17)	0.38625655(66)	2.0672(57)	3.07(13)	0.64	75/80	P56/R46	14	
$^{14}N_2{}^{17}O$											
1003e-0000e	(14 0 3)	7749.64347(21)	7749.64347(21)	0.3949679(17)	1.683(20)	3.77(63)	0.67	38/58	P40/R44	14	12

Notes

The confidence interval (1SD) is in the units of the last quoted digit.

[a] $V_1\ V_2\ l_2\ V_3$ correspond to the maximum value of the modulo of the expansion coefficients of the eigenfunction. V_2 is given between parenthesis when it is larger than 10.

[b] Cluster labelling notation: (P=2V_1+V_2+4V_3, l_2, i), i is the order number within the cluster increasing with the energy.

[c] $\Delta G_v = G_v' - G_v''$ is the band center.

[d] Root Mean Square of the (Obs.-Calc.) differences of the position values (10^{-3} cm^{-1}).

[e] N_{fit} is the total number of transitions included in the fit; N_{obs} is the total number of measured transitions of the considered band.
[f] Observed branch with the maximum value of the total angular momentum quantum number of the input data.
[g] $\Delta P = P' - P''$, where P' and P'' are the upper and lower polyads.
[h] *Notes:*

1- The line positions were included in the fit from Ref. [5];
2- Intrapolyad anharmonic resonance (16 0 7)↔(16 0 6) (J_{cross}=32);
3- Intrapolyad anharmonic resonance (16 0 7)↔ (16 0 6) (J_{cross}=32);
4 -Interpolyad Coriolis resonance (16 2 7)↔(15 1 13) (J_{cross}= e: 32, J_{cross}= f: 32);
5- The line positions were included in the fit from Ref. [8];
6- Intrapolyad anharmonic resonance (15 1 7)↔(15 1 8) (J_{cross}= e: 46, J_{cross}= f: 40);
7- Intrapolyad anharmonic +*l*-type resonance (16 0 10)↔(16 2 16) (J_{cross}=26);
8- Intrapolyad anharmonic (16 0 10)↔(16 0 9) (J_{cross}=49);
9- Intrapolyad anharmonic +*l*-type (16 0 10)↔ (16 2 16) (J_{cross}=26);
10- Intrapolyad anharmonic resonance +*l*-type (14 0 5) ↔ (14 2 12) (J_{cross}=34);
11- Intrapolyad anharmonic resonance (14 0 7)↔(14 0 6) (J_{cross}=35);
Intrapolyad anharmonic +*l*-type resonance (14 0 7)↔(14 2 11) (J_{cross}=48);
12- Intrapolyad anharmonic resonance (14 0 3) ↔(14 0 2) (J_{cross}=70);

[k] Band name as presented in Ref. [7];
[l] Band center as provided by the global effective Hamiltonian.
[m] Vibrational term value as provided by the global effective Hamiltonian.